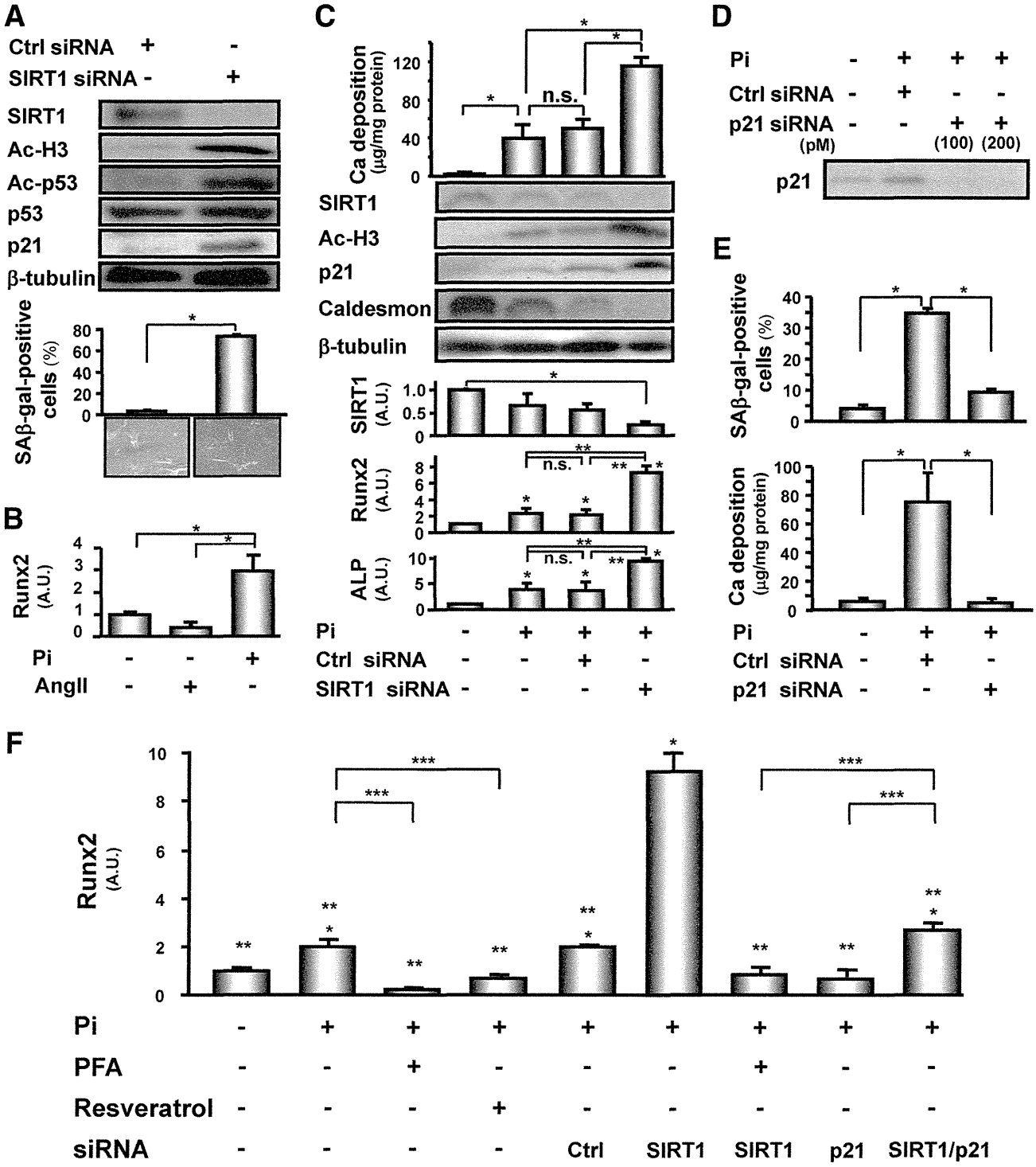

Figure 5. Augmentation of senescence-related smooth muscle cell (SMC) calcification by sirtuin 1 (SIRT1) knockdown in association with osteoblastic phenotypic change and prevention of inorganic phosphate (Pi)–induced changes by p21 knockdown. A, To achieve SIRT1 knockdown in human aortic SMCs (HASMCs), small interfering RNA (siRNA) was simultaneously administered at the start of Pi stimulation (2.6 mmol/L). Complete inhibition of SIRT1 showed a significant increase in acetylation of both substrates (acetylated [Ac]-H3 and Ac-p53), p21 expression and senescence-associated β-galactosidase (SAβ-gal)-positive cells. B, Angiotensin II (Ang II) alone (10 pmol/L) did not increase the expression of Runx2 in the absence of Pi stimulation, unlike Pi stimulation. C, top: SIRT1 knockdown by siRNA significantly accelerated Pi-induced calcification (n=6), whereas control (Ctrl) siRNA did not. C, middle and bottom: Western blots showed that Pi partially inhibited the expression of a differentiated SMC marker, caldesmon, and complete knockdown of SIRT1 by siRNA augmented its downregulation. Real-time polymerase chain reaction analysis showed that Pi induced the expression of Runx-2 and alkaline phosphatase (ALP). Complete knockdown of SIRT1 significantly accelerated the Pi-induced osteoblastic markers. A.U. indicates arbitrary units. *$P<0.05$. D and E, Knockdown of p21 by siRNA (200 pmol/L) significantly reduced the senescent phenotypic change and subsequent calcification (n=6). F, The role of SIRT1/p21 axis in Na-dependent phosphate cotransporter-mediated Runx2 expression was evaluated. Augmentation of Pi-induced Runx2 expression by SIRT1 knockdown was significantly inhibited by double knockdown of SIRT1 and p21. *$P<0.05$ vs control without Pi stimulation (left column), **$P<0.05$ vs Pi-stimulated cells with SIRT1 siRNA (sixth column from left).

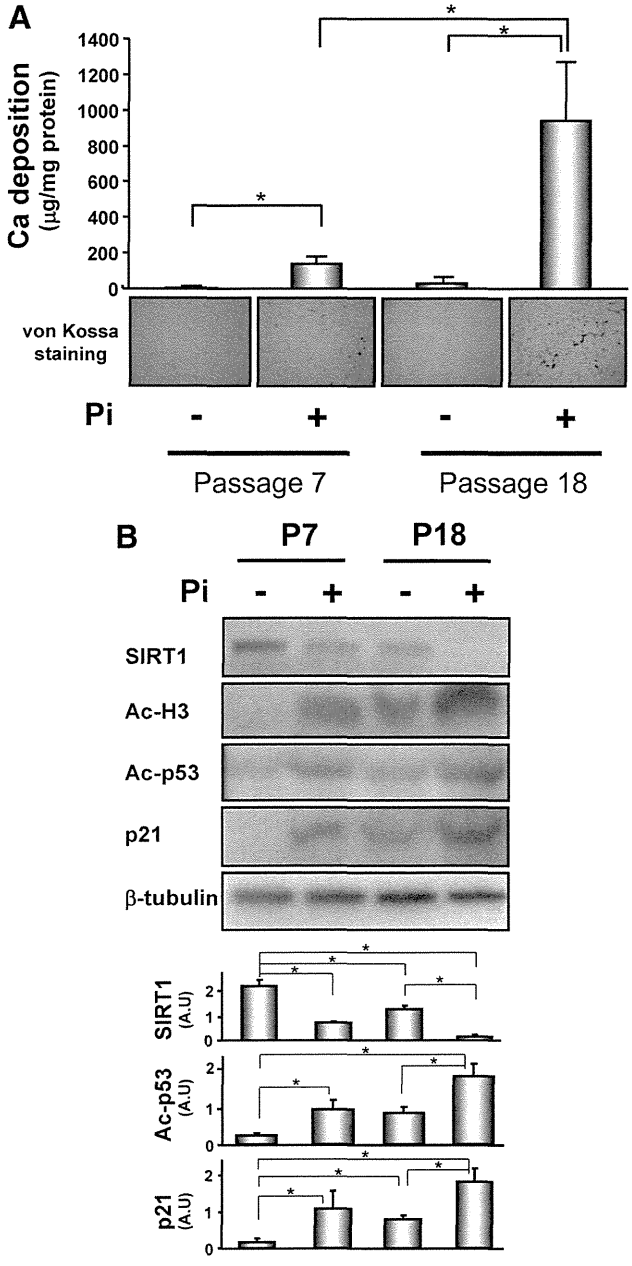

Figure 6. High sensitivity of smooth muscle cells (SMCs) with replicative senescence to inorganic phosphate (Pi)–induced calcification. The effects of replicative senescence in human aortic SMCs (HASMCs) on Pi-induced calcification (A) and sirtuin 1 (SIRT1)-related molecules (B) were also evaluated. A, Senescent cells (passage 18 [P18]) were more sensitive to Pi-induced calcification compared with young cells (passage 7 [P7]) (n=6). Representative photographs of von Kossa staining (bottom) show strong induction of calcium deposition by Pi (2.6 mmol/L). B, Senescent HASMCs (P18) showed a decline in SIRT1 expression and an increase in p21 expression compared with young cells (P7). Pi stimulation of senescent cells significantly inhibited SIRT1 expression and accelerated the increase in p21 and acetylated (Ac)-p53. Densitometric analysis confirmed these more sensitive responses in senescent cells. A.U. indicates arbitrary units. *$P<0.05$.

Second, we also confirmed the association of Pi-induced SMC senescence with calcification in in vitro experiments. Senescent SMCs were significantly increased by Pi even on day 1, although calcium deposition was not markedly increased at the same time point. A statistically significant increase in calcium deposition was found from day 3 and later. Considering these data, we hypothesize that (1) calcium deposition may be more readily induced in senescent cells compared with nonsenescent cells, and (2) Pi-induced senescent change is observed earlier than calcium deposition. In other words, senescent transition associated with Runx2 induction may lead to progressive calcification.

Senescent SMCs were associated with the SIRT1-related p53/p21 pathway, based on the findings that SIRT1 knockdown augmented not only cellular senescence but also calcification. In addition, p21 knockdown completely inhibited senescence-related calcification induced by Pi. This raises the question of how cellular senescence in SMCs is associated with calcification. Our experiments to understand the detailed mechanisms by which SIRT1 modulates senescence-related calcification showed that Pi-induced SIRT1 downregulation led to the phenotypic change from a differentiated state to osteoblast-like cells in SMCs. It has been reported that Pi induces osteoblastic change, in which NPC plays a role in inducing Runx2/Cbfa-1 expression, in SMCs.[17] As the next step, to determine how SIRT1 regulates NPC-mediated Runx2 expression, we examined the effects of knockdown of SIRT1, p21, or both by siRNA on Pi-induced Runx2 expression. Our data shown in Figure 5F suggested that (1) NPC plays an essential role in Pi-induced Runx2 expression, (2) SIRT1 has an inhibitory effect on NPC-mediated Runx2 expression, (3) knockdown of p21 alone ameliorates Runx2 induction, and (4) p21-related osteoblastic change is at least in part dependent on SIRT1.

There is now the new question of how SIRT1 regulates Runx2 regulation. A report by Jeon[18] has shown that acetylation of Runx2 itself is important in osteoblast differentiation, and it is downregulated by HDAC activities. Based on this evidence, SIRT1, 1 of the HDACs, may be able to deacetylate Runx2, leading to inhibition of Runx2-related osteoblastic transition in SMCs. Therefore, the inhibition of SIRT1 by hyperphosphatemia may lead to Runx2 activation via its hyperacetylation. Further investigation of the detailed mechanism of the SIRT1/p21/osteoblastic gene axis is needed. These data clearly suggest that SIRT1 activation may inhibit the hyperphosphatemia-induced osteoblastic phenotypic change of SMCs, and the degree of change may be dependent on SIRT1 expression level. It is possible that the inhibition of SIRT1 expression by Pi alone is "partial," because complete downregulation of SIRT1 by siRNA worsened the dynamic phenotypic change compared with Pi only. We have already shown that tumor necrosis factor-α, a potent atherogenic cytokine, augmented Pi-induced SMC calcification, as previously described.[19] In addition, tumor necrosis factor-α significantly decreased Pi-induced SIRT1 downregulation further (data not shown). According to these results, we currently hypothesize that hyperphosphatemia induces SIRT1 downregulation and subsequent osteoblastic phenotypic change in SMCs, leading to calcification, and these changes are worsened by some harmful atherogenic factors, which decrease SIRT1 expression/activity further. These results provide a new insight, showing that SIRT1 plays an essential role in the prevention of arterial calcification and that the beneficial effect may be associated with an inhibition in Pi-induced SMC senescent transition.

In addition, Ang II did not increase calcium deposition, although the stimulation increased the number of senescent cells. Of note, Ang II alone did not increase Runx2 expression in the absence of Pi (Figure 5B). This result suggests that SMC senescence shows two different features: one is SAβ-gal-positive cells with an increase in Runx2 and the other is SAβ-gal-positive cells without. First, it has recently been reported that SMCs with replicative senescence, rather than the cells without senescence, show hypersensitivity in response to induction of calcification with the more induction of osteoblastic markers,[20] suggesting that the induction of osteoblastic transdifferentiation is strongly associated with the senescent change in SMCs. In addition, the translocation of SIRT1 to cytoplasm was observed after Pi stimulation for 24 hours, although SIRT1 predominantly localized in nucleus without Pi. In contrast, Ang II did not show the dynamic translocation. Thinking about the mechanism for regulating the activity of HDACs, including SIRT1, recent several reports show the importance of their coordinated shuttling between nucleus and cytoplasm. A report demonstrates that HDAC7, an HDAC, represses the transcriptional activity of Runx2 and that osteogenic stimuli induce export of HDAC7 from nucleus, leading to a decline in the repressive potentials of HDAC7 for Runx2.[21] On the basis of our findings and a previous report, the reason that stimulation with Ang II alone did not induce Runx2 expression and subsequently SMC calcification may in part depend on the difference of SIRT1 translocation after stimulation. Therefore, we strongly hypothesize that in the senescent SMCs with upregulation of p21, Pi stimulation, but not Ang II stimulation, may activate Runx2 via at least two phenomena, the hyperacetylation of Runx2 by SIRT1 downregulation and the dynamic SIRT1 translocation, leading to marked osteoblastic transdifferentiation and subsequent calcification. In addition, we have another hypothesis. In general, it has been shown that high-dose Pi navigates release of matrix vesicles from SMCs in parallel with osteoblastic transdifferentiation. The vesicles play an essential role in the initiation of hydroxyapatite aggregation, so-called nucleation. Accumulating recent reports show that the nanocrystal formation as an initial step under hyperphosphatemia accelerates the harmful cascade of osteoblastic transdifferentiation in SMCs via endocytosis.[22,23] Maybe Ang II alone does not induce the nanocrystal formation and the cascade of osteoblastic change. Therefore, we explain that the difference of senescent phenotypic changes in SMCs between both stimulations, Pi and Ang II alone, may depend on (1) SIRT1 translocation and (2) nanocrystal formation to accelerate calcification. Further investigation to address the detailed mechanisms by which SIRT1 regulates osteoblastic transdifferentiation in SMCs under the cellular senescence is needed.

Are SIRT1 downregulation-related SMC senescence and subsequent calcification reversible or not? To answer this question, the effects of continuation or termination of high-dose Pi were examined. As shown in Figure 3B, termination (on day 6) of Pi showed no progression of senescence-related calcification in association with the restoration of SIRT1, whereas continuation (up to day 10) of Pi stimulation showed further progression of calcification. It is suggested that a therapeutic strategy to manage hyperphosphatemia to the normal range of serum phosphate concentration may lead to at least termination of progressive calcification via reversal of SIRT1 activity.

Cellular senescence has been shown to have two features: not only stress-induced premature senescence but also replicative senescence, indicating a limited number of divisions in culture.[24] In fact, both endothelial cells and SMCs derived from human atherosclerotic plaques show a senescent phenotype earlier than do cells from normal vessels.[25] Notably, we found that senescent HASMCs were significantly more sensitive to Pi-induced calcification compared with young cells. These results suggest that calcium deposition may be more readily induced in arterial medial SMCs with replicative senescence. This insight may explain the mechanisms by which arterial calcification occurs in the elderly more frequently than in the young population. Therefore, these observations support our hypothesis that arterial calcification is accelerated by both senescent types (premature and replicative senescence) in SMCs. To explore new therapeutic strategies against arterial calcification, it is essential to investigate how to maintain a higher SIRT1 level in the vasculature, leading to prevention of medial SMC senescence and which drug is capable of achieving it.

How does SIRT1 exert protective effects against SMC calcification? This study clearly showed that inhibition of SIRT1 was associated with increases in both Ac-p53 and p21 expression. These findings were significantly induced by not only replicative senescence but also Pi-induced premature senescence. SIRT1-mediated deacetylation of p53 inhibits p53-dependent transactivation of target genes, including p21. A report showed that a decline in cellular deacetylase activity increases the half-life of endogenous p53,[26] suggesting that p53 acetylation is also associated with p53 stabilization. Therefore, the increased Ac-p53 by Pi-induced SIRT1 downregulation may induce SMC senescence because of a decline in degradation of p53, leading to calcification. In addition, p53 itself can inhibit SIRT1 transcription because the SIRT1 promoter has two response elements to p53.[27] Further investigation to address how the SIRT1-p53 negative regulatory pathway is associated with SMC calcification is needed.

On the other hand, regarding p21 activation, it is reported that inhibition of p21 expression in the vasculature significantly attenuates cellular senescence, leading to prevention of atherosclerosis.[28] This evidence suggests a pivotal role of p21 in the development of atherosclerosis. p21 activation has been shown to be regulated by a pathway that is p53 dependent, p53 independent, or both. Okamoto et al have demonstrated that inhibition of HDAC by trichostatin A showed activation of p21 promoter activity by the Sp1 site even in vascular SMCs, and the induction of p21 was independent of the p53 pathway.[29] The p21 transcriptional activation in response to HDAC inhibitors was mediated by histone hyperacetylation in its promoter region. Based on these findings, Pi-induced p21 activation via SIRT1 downregulation may be in part involved in a p53-independent pathway, leading to a senescent phenotype of SMCs. Further investigation exploring which molecule activates the p21 promoter under hyperphosphatemia is needed.

Conclusion

We showed that SIRT1 exerts a protective role in hyperphosphatemia-based arterial calcification via inhibition of osteoblastic transdifferentiation, in association with cross-talk between calcification and cellular senescence. This ability of SIRT1 may orchestrate an analogous protective/longevity paradigm even in vascular SMCs, leading to maintenance of healthy elasticity of the arterial wall. Strategies to maintain a higher level of SIRT1 activity may provide novel therapeutic opportunities for the prevention of arterial calcification.

Acknowledgments

This study was supported by Grants-in-Aid for Scientific Research from the Ministry of Education, Science, Culture and Sports of Japan (No. 19590854, No. 21590947, and No. 20249041), Ono Medical Research Foundation, Kanzawa Medical Research Foundation, Novartis Foundation for Gerontological Research, Takeda Research Foundation, and Mitsui-Sumitomo Insurance Welfare Foundation.

Sources of Funding

This manuscript is supported by Grants-in-Aid for Scientific Research from the Ministry of Education, Science, Culture and Sports of Japan (No. 19590854, No. 21590947, No. 20249 041). In particular, this is mainly supported by No. 21590947.

Disclosures

None.

References

1. Safar ME, Levy BI, Struijker-Boudier H. Current perspectives on arterial stiffness and pulse pressure in hypertension and cardiovascular diseases. *Circulation.* 2003;107:2864–2869.
2. Abedin M, Tintut Y, Demer LL. Vascular calcification: mechanisms and clinical ramifications. *Arterioscler Thromb Vasc Biol.* 2004;24:1161–1170.
3. Iijima K, Hashimoto H, Hashimoto M, Son BK, Ota H, Ogawa S, Eto M, Akishita M, Ouchi Y. Aortic arch calcification detectable on chest X-ray is a strong independent predictor of cardiovascular events beyond traditional risk factors. *Atherosclerosis.* 2010;210:137–144.
4. Demer LL, Tintut Y. Vascular calcification: pathobiology of a multifaceted disease. *Circulation.* 2008;117:2938–2948.
5. Ehara S, Kobayashi Y, Yoshiyama M, Shimada K, Shimada Y, Fukuda D, Nakamura Y, Yamashita H, Yamagishi H, Takeuchi K, Naruko T, Haze K, Becker AE, Yoshikawa J, Ueda M. Spotty calcification typifies the culprit plaque in patients with acute myocardial infarction: an intravascular ultrasound study. *Circulation.* 2004;110:3424–3429.
6. Shroff RC, Shanahan CM. The vascular biology of calcification. *Semin Dial.* 2007;20:103–109.
7. Persy V, D'Haese P. Vascular calcification and bone disease: the calcification paradox. *Trends Mol Med.* 2009;15:405–416.
8. Shanahan CM, Cary NR, Salisbury JR, Proudfoot D, Weissberg PL, Edmonds ME. Medial localization of mineralization-regulating proteins in association with Monckeberg's sclerosis: evidence for smooth muscle cell-mediated vascular calcification. *Circulation.* 1999;100:2168–2176.
9. Tyson KL, Reynolds JL, McNair R, Zhang Q, Weissberg PL, Shanahan CM. Osteo/chondrocytic transcription factors and their target genes exhibit distinct patterns of expression in human arterial calcification. *Arterioscler Thromb Vasc Biol.* 2003;23:489–494.
10. Brachmann CB, Sherman JM, Devine SE, Cameron EE, Pillus L, Boeke JD. The SIR2 gene family, conserved from bacteria to humans, functions in silencing, cell cycle progression, and chromosome stability. *Genes Dev.* 1995;9:2888–2902.
11. Vaziri H, Dessain SK, Ng Eaton E, Imai SI, Frye RA, Pandita TK, Guarente L, Weinberg RA. hSIR2(SIRT1) functions as an NAD-dependent p53 deacetylase. *Cell.* 2001;107:149–159.
12. Langley E, Pearson M, Faretta M, Bauer UM, Frye RA, Minucci S, Pelicci PG, Kouzarides T. Human SIR2 deacetylates p53 and antagonizes PML/p53-induced cellular senescence. *EMBO J.* 2002;21:2383–2396.
13. Ota H, Akishita M, Eto M, Iijima K, Kaneki M, Ouchi Y. Sirt1 modulates premature senescence-like phenotype in human endothelial cells. *J Mol Cell Cardiol.* 2007;43:571–579.
14. Yokozawa T, Zheng PD, Oura H, Koizumi F. Animal model of adenine-induced chronic renal failure in rats. *Nephron.* 1986;44:230–234.
15. Son BK, Kozaki K, Iijima K, Eto M, Kojima T, Ota H, Senda Y, Maemura K, Nakano T, Akishita M, Ouchi Y. Statins protect human aortic smooth muscle cells from inorganic phosphate-induced calcification by restoring Gas6-Axl survival pathway. *Circ Res.* 2006;98:1024–1031.
16. Ferrari AU, Radaelli A, Centola M. Invited review: aging and the cardiovascular system. *J Appl Physiol.* 2003;95:2591–2597.
17. Jono S, McKee MD, Murry CE, Shioi A, Nishizawa Y, Mori K, Morii H, Giachelli CM. Phosphate regulation of vascular smooth muscle cell calcification. *Circ Res.* 2000;87:E10–E17.
18. Jeon EJ, Lee KY, Choi NS, Lee MH, Kim HN, Jin YH, Ryoo HM, Choi JY, Yoshida M, Nishino N, Oh BC, Lee KS, Lee YH, Bae SC. Bone morphogenetic protein-2 stimulates Runx2 acetylation. *J Biol Chem.* 2006;281:16502–16511.
19. Son BK, Akishita M, Iijima K, Kozaki K, Maemura K, Eto M, Ouchi Y. Adiponectin antagonizes stimulatory effect of tumor necrosis factor-α on vascular smooth muscle cell calcification: regulation of growth arrest-specific gene 6-mediated survival pathway by adenosine 5′-monophosphate-activated protein kinase. *Endocrinology.* 2008;149:1646–1653.
20. Nakano-Kurimoto R, Ikeda K, Uraoka M, Nakagawa Y, Yutaka K, Koide M, Takahashi T, Matoba S, Yamada H, Okigaki M, Matsubara H. Replicative senescence of vascular smooth muscle cells enhances the calcification through initiating the osteoblastic transition. *Am J Physiol Heart Circ Physiol.* 2009;297:H1673–H1684.
21. Jensen ED, Gopalakrishnan R, Westendorf JJ. Bone morphogenic protein 2 activates protein kinase D to regulate histone deacetylase 7 localization and repression of Runx2. *J Biol Chem.* 2009;284:2225–2234.
22. Ewence AE, Bootman M, Roderick HL, Skepper JN, McCarthy G, Epple M, Neumann M, Shanahan CM, Proudfoot D. Calcium phosphate crystals induce cell death in human vascular smooth muscle cells: a potential mechanism in atherosclerotic plaque destabilization. *Circ Res.* 2008;103:e28–e34.
23. Sage AP, Lu J, Tintut Y, Demer LL. Hyperphosphatemia-induced nanocrystals upregulate the expression of bone morphogenetic protein-2 and osteopontin genes in mouse smooth muscle cells in vitro. *Kidney Int.* 2011;79:414–422.
24. Hayflick L. Current theories of biological aging. *Fed Proc.* 1975;34:9–13.
25. Minamino T, Komuro I. Vascular cell senescence: contribution to atherosclerosis. *Circ Res.* 2007;100:15–26.
26. Ito A, Lai CH, Zhao X, Saito S, Hamilton MH, Appella E, Yao TP. p300/CBP-mediated p53 acetylation is commonly induced by p53-activating agents and inhibited by MDM2. *EMBO J.* 2001;20:1331–1340.
27. Nemoto S, Fergusson MM, Finkel T. Nutrient availability regulates SIRT1 through a forkhead-dependent pathway. *Science.* 2004;306:2105–2108.
28. Andreassi MG. DNA damage, vascular senescence and atherosclerosis. *J Mol Med.* 2008;86:1033–1043.
29. Okamoto H, Fujioka Y, Takahashi A, Takahashi T, Taniguchi T, Ishikawa Y, Yokoyama M. Trichostatin A, an inhibitor of histone deacetylase, inhibits smooth muscle cell proliferation via induction of p21(WAF1). *J Atheroscler Thromb.* 2006;13:183–191.

Supplement Material

Sirtuin SIRT1 retards hyperphosphatemia-induced calcification of vascular smooth muscle cells

Methods

Aortic calcification in renal failure rats

Renal failure was induced in rats by a 0.75% adenine-containing diet as previously described.[28] Twelve-week-old male Wistar rats (Nippon Clea Inc., Japan) were pair-fed standard CE-2 chow (containing 1.2% calcium and 0.6% phosphorus; Nippon Clea Inc.) in the control group or CE-2 chow containing 0.75% adenine (Sigma) in the renal failure group for 4 weeks. Then, the diet was returned to normal chow for an additional 4 weeks. After induction of renal failure for 8 weeks in total, the rats were sacrificed to collect samples. After perfusion with saline at a constant, nonpulsatile pressure of 100 mmHg, the aorta was immediately embedded in OCT compound frozen section and sequentially cut into cross-sections with 5-μm thickness from each part of the aorta. To detect calcification in the aortic wall, each cross-section was subjected to von-Kossa staining to demonstrate mineralization. The calcified area and number of

SAβ-gal-positive cells in the cross-section were measured by image analysis software (ImageJ, Scion Image, Maryland, USA). All procedures and animal care were in accordance with the Guide for the Care and Use of Laboratory Animals of the University of Tokyo.

Induction of SMC calcification

Primary human aortic SMC (HASMC), derived from the internal thoracic artery (Clonetics), were treated with a pathological concentration of inorganic phosphate (Pi) in culture medium. To set up the calcification medium, a mixed solution of Na_2HPO_4 and NaH_2PO_4 whose pH was adjusted to 7.4 was added to serum-supplemented DMEM to final doses of up to 3.2 mmol/L as previously described.[29] To quantitatively measure Pi-induced calcification, two distinct experiments, (1) intracellular calium (Ca) deposition as determined by *o*-cresolphthalein complexone method and (2) visualization of mineralization as determined by von-Kossa staining, were performed as previously described.[28] We have previously confirmed that excessive Pi stimulation dose- and time-dependently induced calcium deposition in HASMC, whereas a normal Pi dose (1.4 mmol/L), equivalent to the human physiological level of serum phosphate, did not.[29]

Senescence-associated β-galactosidase (SAβ-gal) staining

To assess senescent changes in the phenotype of cultured HASMC or aortic medial cells of rats with/without renal failure, staining for senescence-associated β-galactosidase (SAβ-gal), a well-established biomarker of cellular senescence, was performed at pH 6.0, as opposed to endogenous lysosomal enzyme detected at pH 4.0 in normal cells, as previously described.[30] Numbers of SAβ-gal-positive cells were quantitatively counted in the aortic wall or cultured HASMC. As a positive control in *in vitro* experiments, angiotensin II (AngII) was used to induce transition to a senescent phenotype in HASMC.

Knockdown of SIRT1 or p21 by small interfering RNA

HASMC were transfected with 200 pmol/L small interfering RNA (siRNA) for SIRT1 (GAT GAA GTT GAC CTC CTC A and TGA AGT GCC TCA GAT ATT A, Santa Cruz Biotechnology) or control (Cntl) using silMPORTER (Upstate). In addition, knockdown of $p21^{WAF1/CIP1}$ was performed using 100 to 200 pmol/L siRNA for p21 (CGA CUG UGA UGC GCU AAU G, CCU AAU CCG CCC ACA GGA A, CGU CAG AAC CCA UGC GGC A, and AGA CCA GCA UGA CAG AUU U) by the same

method. To inhibit p21 expression effectively and completely, four kinds of sequences of p21 siRNA were used. HASMC were treated simultaneously with these siRNAs at the start of Pi stimulation.

Western blot and SDS-PAGE

Protein expression was assessed by Western blot analysis with chemiluminescence detection. SIRT1 was detected using a rabbit polyclonal anti-SIRT1 antibody (Abcam), and p53, acetylated p53 (Ac-p53; Lys-382), acetylated histone-3 (Ac-H3), p21, caldesmon and β-tubulin were detected with monoclonal antibodies (Santa Cruz Biotechnology). The expression levels of Ac-p53 and Ac-H3 were used to reflect SIRT1 activity as a deacetylase. Caldesmon was used to reflect a lineage marker of SMC differentiation.

Real-time PCR analysis: Osteoblastic markers

Primer sequences were as follows:

ALP; (forward) ACCATTCCCACGTCTTCACATTTG,

(reverse) AGACATTCTCTCGTTCACCGCC,

Runx-2/Cbfa-1; (forward) TCTGGCCTTCCACTCTCAGT,

(reverse) GACTGGCGGGGTGTAAGTAA,

SIRT1; (forward) CCTGACTTCAGGTCAAGGGATGGTA,

(reverse) CTGATTAAAAATATCTCCTCGTACAG,

β-actin; (forward) CTGGAACGGTGAAGGTGACA,

(reverse) AAGGGACTTCCTGTAACAATGC.

Materials

Angiotensin II (AngII) was used to induce senescent phenotypic change in cultured HASMC as a positive control. To inhibit activity of Na-dependent phosphate cotransporter (NPC) stimulated by treatment with exogenous Pi, phosphonoformic acid (PFA; SIGMA), a chemical inhibitor, was used. Sirtinol (a chemical inhibitor; Calbiochem) or resveratrol (an activator of SIRT1; WAKO) was used for modulation of SIRT1 activity. Localization of SIRT1 in HASMC was detected using its antibody (Santa Cruz: sc-15404).

Immunohistological staining

To address a difference in senescent induction by Pi or AngII, the localization of SIRT1 in HASMC was compared using immunohistological assessment. SIRT1 specific

antibody showed localization and its translocation in HSMC before or after stimulation of Pi alone (2.6 mM) or AngII alone (10 pmol/L). Nucleus was detected by DAPI stain.

Statistical analysis

All results are presented as mean ± standard error (SE). Differences between the groups were analyzed using ANOVA, followed by Fisher's PLSD test. A value of $P < 0.05$ was considered to be significant. All *in vitro* experiments were performed at least three times.

Figure legends

Supplemental figure 1. Deterioration of osteoblastic transition by SIRT1 knockdown under high-dose Pi stimulation

The effect of SIRT1 knockdown on osteoblastic markers, Runx2 and ALP, in the condition of normal Pi or high-dose Pi was examined. Complete knockdown of SIRT1 showed significantly augmented expression of both osteoblastic markers, Runx2 and ALP, in a high-dose Pi condition; however, augmentation was not found in a normal Pi condition. These data suggest that intracellular Pi influx by Pi stimulation is essential to

induce SMC calcification in association with osteoblastic phenotypic change, and the osteoblastic transition may be correlated with NPC, a cotransporter of Pi.

Supplemental figure 2. Translocation of SIRT1 in HASMC is induced by Pi, but not AngII.

To address a difference in senescent induction by Pi or AngII, immunohistological assessment of SIRT1 in HASMC was examined. SIRT1 was predominantly localized in nucleus without Pi. Dynamic translocation of SIRT1 to cytoplasm was observed after Pi stimulation (2.6 mM) for 24 hr and its expression disappeared in both areas on day 6. In contrast, AngII alone (10 pmol/L) did not show the dynamic translocation. SIRT1 siRNA shows complete knockdown of SIRT1 expression. DAPI shows nuclear stain.

Supplement Material Figure I

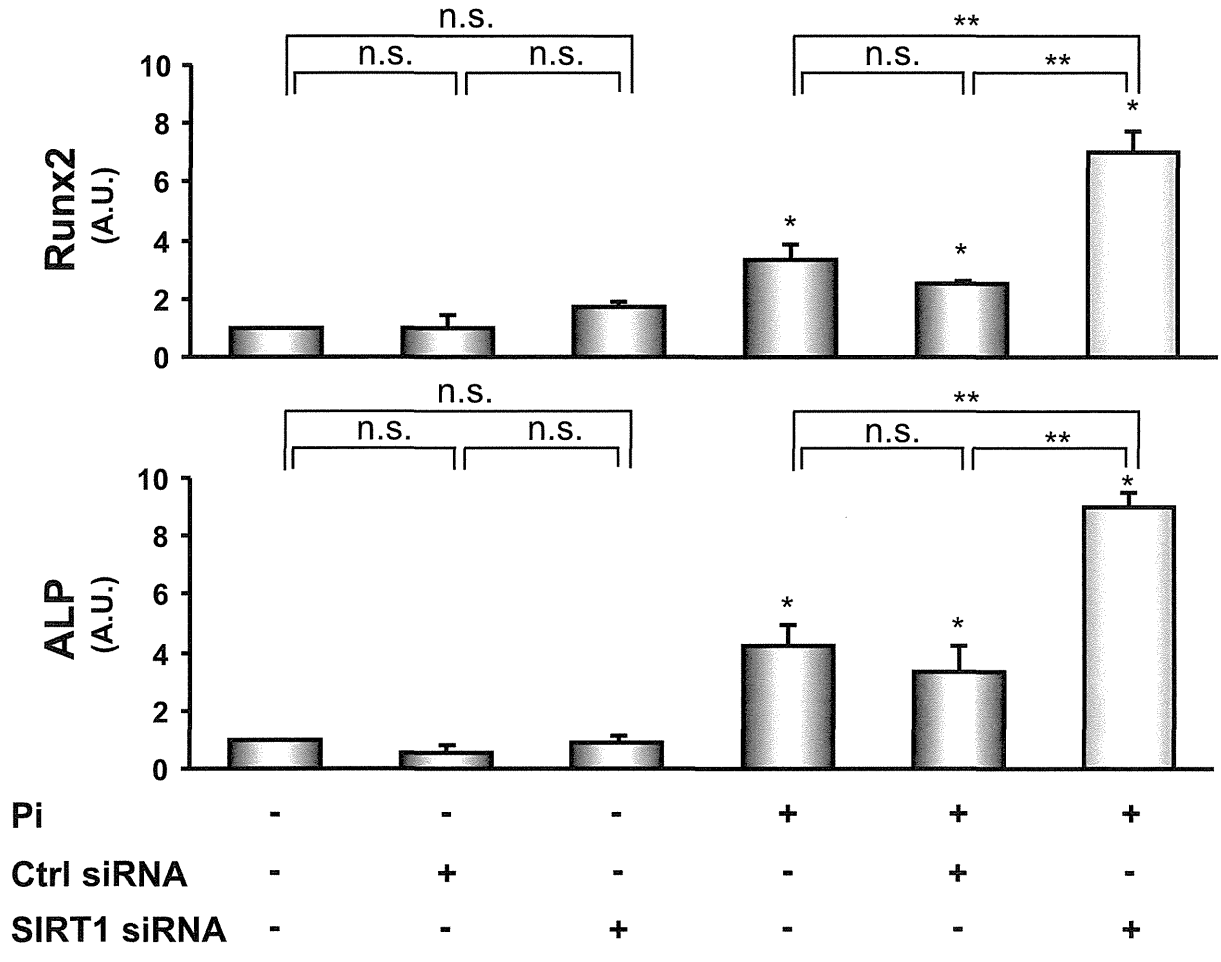

Supplement Material Figure II

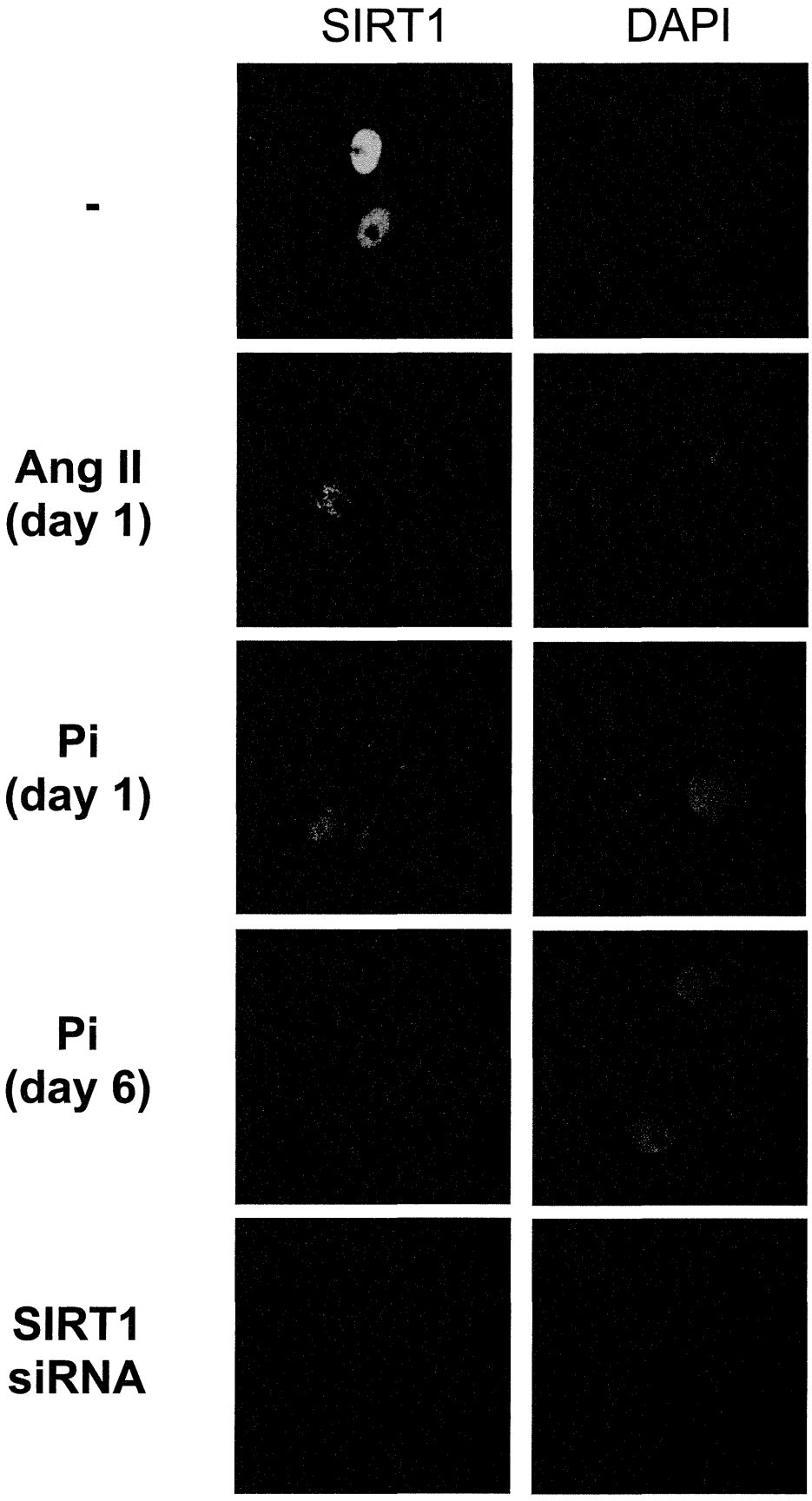

Bruno Fantino, MD, PhD
Medical School
University of Angers
UNAM
Angers, France
Department of Geriatrics
Angers University Hospital
Angers, France

Laure De Decker, MD, MS
Medical School
University of Nantes
UNAM
Nantes, France
Department of Geriatrics
Nantes University Hospital
Nantes, France

Olivier Beauchet, MD, PhD
Cédric Annweiler, MD, PhD
Medical School
University of Angers
UNAM
Angers, France
Department of Geriatrics
Angers University Hospital
Angers, France

ACKNOWLEDGMENTS

The authors wish to thank Angers University Hospital for technical support.

Conflict of Interest: Prof. Beauchet serves as an unpaid consultant for Ipsen Pharma company and as a board member for Gériatrie, Psychologie et Neuropsychiatrie du Vieillissement. He has no relevant financial interest in this manuscript. Dr. Annweiler serves as an unpaid consultant for Ipsen Pharma Company. He has no relevant financial interest in this manuscript.

Author Contributions: Annweiler had full access to the data in the study and takes responsibility for the integrity of the data and the accuracy of the data analyses. Study concept and design: Annweiler and Beauchet. Acquisition of data: Calès, Redureau, and Abraham. Analysis and interpretation of data: Abraham, Calès, Redureau, Annweiler, and Beauchet. Drafting of the manuscript: Annweiler, Abraham, Beauchet, Calès, and Redureau. Critical revision of the manuscript for important intellectual content: Fantino and De Decker. Statistical expertise: Annweiler. Administrative, technical, or material support: Beauchet. Study supervision: Annweiler.

Sponsor's Role: None.

REFERENCES

1. Melamed ML, Muntner P, Michos ED et al. Serum 25-hydroxyvitamin D levels and the prevalence of peripheral arterial disease: Results from NHANES 2001 to 2004. Arterioscler Thromb Vasc Biol 2008;28: 1179–1185.
2. Barnard K, Colon-Emeric C. Extraskeletal effects of vitamin D in older adults: Cardiovascular disease, mortality, mood, and cognition. Am J Geriatr Pharmacother 2010;8:4–33.
3. Freedman BI, Wagenknecht LE, Hairston KG et al. Vitamin D, adiposity, and calcified atherosclerotic plaque in African-Americans. J Clin Endocrinol Metab 2010;95:1076–1083.
4. Razzaque MS. The dualistic role of vitamin D in vascular calcifications. Kidney Int 2011;79:708–714.
5. Norgren L, Hiatt WR, Dormandy JA et al. Inter-Society Consensus for the management of peripheral arterial disease (TASC II). J Vasc Surg 2007;45: S5–S67.
6. Allison MA, Hiatt WR, Hirsch AT et al. A high ankle-brachial index is associated with increased cardiovascular disease morbidity and lower quality of life. J Am Coll Cardiol 2008;51:1292–1298.
7. Bischoff-Ferrari HA, Giovannucci E, Willett WC et al. Estimation of optimal serum concentrations of 25-hydroxyvitamin D for multiple health outcomes. Am J Clin Nutr 2006;84:18–28.
8. Bas A, Lopez I, Perez J et al. Reversibility of calcitriol-induced medial artery calcification in rats with intact renal function. J Bone Miner Res 2006;21:484–490.
9. Zebger-Gong H, Müller D, Diercke M et al. 1,25-Dihydroxyvitamin D3-induced aortic calcifications in experimental uremia: Up-regulation of osteoblast markers, calcium-transporting proteins and osterix. J Hypertens 2011;29:339–348.
10. Bolland MJ, Avenell A, Baron JA et al. Effect of calcium supplements on risk of myocardial infarction and cardiovascular events: Meta-analysis. BMJ 2010;341:c3691. doi: 10.1136/bmj.c3691.

PULMONARY FEATURES ASSOCIATED WITH BEING UNDERWEIGHT IN OLDER MEN

To the Editor: Body mass index (BMI) is one of the most potent prognostic markers in chronic obstructive pulmonary disease (COPD),[1] but it is unclear whether low body weight worsens the symptoms, respiratory function, and prognosis of COPD or only reflects one aspect of advanced COPD.

It is difficult for people with COPD to differentiate the effects of being underweight on pulmonary symptoms and function from the worsening of COPD itself, because a cachexic state is frequently associated with the advance of COPD. One effective approach to this uncertainty would be to assess the respiratory function and symptoms of people with severely low body weight due to causes not associated with respiratory function.[2] These observations would indicate whether nutritional therapy could mitigate respiratory symptoms and dysfunction in people with COPD.

This report presents a case of an 85-year-old man who underwent total gastrectomy and cholecystectomy because of stomach cancer. He had never smoked and had shown no shortness of breath during exercise. He had mild anemia and was diagnosed with stomach cancer. No major postoperative complications occurred, and he left the hospital 12 days after the surgery, but he had severe loss of appetite and his BMI decreased from 25.0 kg/m^2 before the surgery to 17.2 kg/m^2 5 months after the surgery. Although no pulmonary complications were detected on chest computed tomography, he complained of shortness of breath during light exercise corresponding to Medical Research Council (MRC) dyspnea scale Grade 4. His vital capacity (VC) decreased from 3.04 L before surgery to 1.96 L after, and his forced expiratory volume in 1 second (FEV_1)/VC ratio paradoxically increased from 62.8% to 93.9%, masking the preexisting mild obstructive pulmonary disorder. His residual volume to total lung capacity (RV/TLC) ratio reached 62.6% after the surgery, whereas TLC was 94.0% of the predicted value. No hypoxia was observed despite the severe shortness of breath.

The pulmonary features of older outpatients with severely low body weight without respiratory diseases were

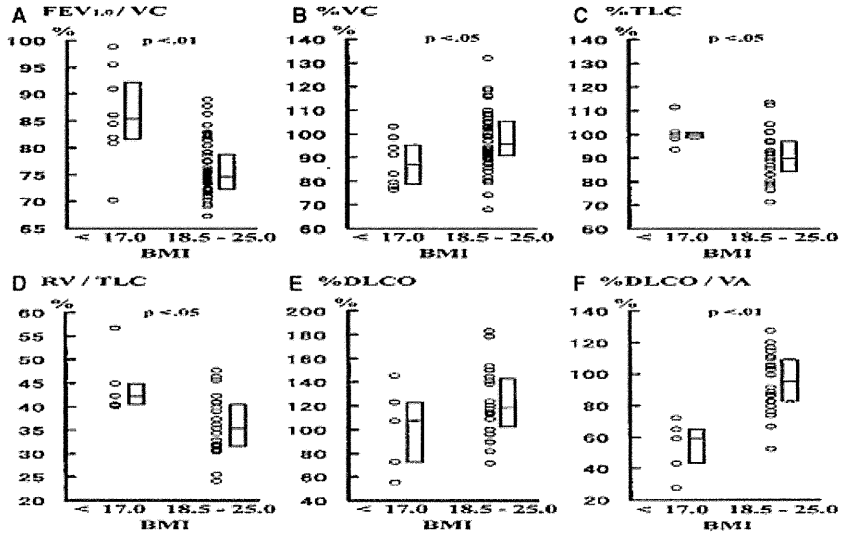

Figure 1. Pulmonary function of underweight patients and normal-weight patients. Ratio of forced expiratory volume in 1 second to VC (FEV_1/VC), percentage of VC (%VC), percentage of TLC (%TLC), residual volume to total lung capacity (RV/TLC) ratio, percentage of diffusing capacity of carbon monoxide (%DLCO), and %DLCO to alveolar volume (%DLCO/VA) of older men with a body mass index (BMI) less than 17.0 kg/m^2 were compared with those of older men with a BMI of 18.5 to 25.0 kg/m^2. Each circular point indicates measured individual data. The boxes indicate the 25th percentile, median, and 75th percentile values. The FEV_1/VC ratio, %TLC, and the RV/TLC ratio were significantly higher, and %VC and %DLCO/VA were significantly lower in the men with BMI < 17.0 kg/m^2.

also investigated. The study population included men aged 65 and older who visited the Department of Geriatric Medicine at the University of Tokyo Hospital from September to October 2008 and men aged 65 and older who visited the Department of Respiratory Medicine at the University of Tokyo Hospital in October 2009. Spirometry had been performed according to Japanese Respiratory Society guidelines.[3] The ethics committee in the medical department at the University of Tokyo approved this study protocol.

The study excluded patients with a FEV_1/FVC ratio of less than 70% or other pulmonary complications observable on chest radiographs or documented in medical records, such as pulmonary malignancies, marked sequelae of pulmonary tuberculosis, interstitial pneumonia, massive pleural effusion, active pneumonia, acute or refractory heart failure, history of lobectomy, and bronchial asthma. Angina pectoris, palpitation, and paroxysmal dyspnea were excluded from the evaluations of respiratory symptoms.

Respiratory symptom and function data were obtained from eight older men with a BMI less than 17.0 kg/m^2. The cause of low body weight of these men were depression (n = 2), a past history of partial or total gastrectomy (n = 3), a past history of ulcerative colitis (n = 1), and no specific diseases (n = 2). Five had shortness of breath when walking up a slight hill, and two complained of shortness of breath even during light exercise, corresponding to MRC dyspnea scale Grades 3 to 4, as observed in the presented case. None had signs of hypoxia at rest.

Data were also obtained from 50 older men with a BMI between 18.5 and 25.0 kg/m^2 (normal weight) without evident pulmonary disease. Only four had shortness of breath during exercise ($P = .001$, Fisher exact test), and none had severe shortness of breath corresponding to MRC dyspnea scale Grade 3 or greater.

The pulmonary function data of the older underweight men without pulmonary diseases (BMI < 17.0 kg/m^2) were compared with those of the older normal-weight men without pulmonary diseases (BMI 18.5–25.0 kg/m^2) using the Mann-Whitney *U* test. DLCO/VA is the ratio of diffusing capacity of carbon monoxide to alveolar volume. Percentage of VC (%VC), percentage of TLC (%TLC), and the percentage of DLCO/VA (%DLCO/VA) were determined by calculating the percentage of individual data to the predicted values; %TLC ($P = .04$) and RV/TLC ratios ($P = .02$) were significantly higher in the underweight men than in those who were normal weight (Figure 1). The %VC and %DLCO/VA was significantly lower in the underweight men than in those who were normal weight (%VC, $P = .04$; %DLCO/VA, $P = .001$; Figure 1). The FEV_1/VC ratio was paradoxically greater in the underweight men, maybe because of the lower VC and higher RV/TLC ratios ($P = .003$).

Being severely underweight involves weakened muscular strength. The higher RV/TLC ratios, lower VC, and higher FEV_1/VC ratios of the older underweight men could be due to the weakened respiratory muscles, especially expiratory muscles.[4] Higher %TLC and lower %DLCO/VA without a concomitant DLCO decrease would indicate lung hyperinflation in the older underweight men. These findings are also consistent with reported lung pathology in starved animals, which shows endogenous alveolar loss without necrosis or inflammation.[5]

These findings support the clinical benefit of promoting nutritional therapy to avoid excessive weight loss in people with COPD and older adults.[6] Further prospective studies evaluating the changes in respiratory symptoms and

function associated with low body weight or alterations in body composition are warranted.

Yasuhiro Yamaguchi, MD
Shinicihiro Hibi, MD
Masaki Ishii, MD
Yoko Hanaoka, MD
Department of Geriatric Medicine

Hidenori Kage, MD
Department of Respiratory Medicine

Hiroshi Yamamoto, MD
Department of Geriatric Medicine
Yasuhiro Yamauchi, MD
Department of Respiratory Medicine

Masato Eto, MD
Department of Geriatric Medicine

Takahide Nagase, MD
Department of Respiratory Medicine

Yasuyoshi Ouchi, MD
Department of Geriatric Medicine
Graduate School of Medicine
University of Tokyo
Tokyo, Japan

ACKNOWLEDGMENTS

This work was supported by grants-in-aid for young scientists from the Ministry of Education, Science, Sports and Culture of Japan.

Conflict of Interest: No conflicts of interest to disclose.

Author Contributions: Yasuhiro Yamaguchi: coordinator of study concept and design, data analysis, preparation of manuscript. Shinnicihiro Hibi: acquisition of data. Masaki Ishii and Yoko Hanaoka: data analysis. Hidenori Kage: data analysis and preparation of manuscript. Hiroshi Yamamoto: interpretation of data. Yasuhiro Yamauchi: acquisition of data and subjects. Masato Eto: interpretation of data. Takahide Nagase: coordinator of study concept and design. Yasuyoshi Ouchi: coordinator of study concept and design.

Sponsor's Role: None.

REFERENCES

1. Celli BR, Cote CG, Marin JM et al. The body-mass index, airflow obstruction, dyspnea, and exercise capacity index in chronic obstructive pulmonary disease. N Engl J Med 2004;350:1005–1012.
2. Gardini Gardenghi G, Boni E, Todisco P et al. Respiratory function in patients with stable anorexia nervosa. Chest 2009;136:1356–1363.
3. Tamura G, Aizawa H, Nagai A et al. Common prediction equations of respiratory function tests from children to adults in Japan. Nihon Kokyuki Gakkai Zasshi 2007;45:526–542.
4. Kreitzer SM, Saunders NA, Tyler HR et al. Respiratory muscle function in amyotrophic lateral sclerosis. Am Rev Respir Dis 1978;117:437–447.
5. Massaro D, Massaro GD, Baras A et al. Calorierelated rapid onset of alveolar loss, regeneration, and changes in mouse lung gene expression. Am J Physiol 2004;286:L896–L906.
6. Feldblum I, German L, Castel H et al. Individualized nutritional intervention during and after hospitalization: The Nutrition Intervention Study clinical trial. J Am Geriatr Soc 2011;59:10–17.

LIVING WITH STAIRS: FUNCTIONING IN A LARGE COHORT OF OLDER AUSTRALIAN ADULTS

To the Editor: Stair climbing has been encouraged as a health promotion measure in the general population,[1] and health benefits have been demonstrated in young people,[2] but these benefits may not extend to older adults, and living in a building with stairs may prove challenging for older adults. The difficulty that older adults experience in climbing up or down stairs has been associated with a number of chronic conditions, including hypertension, arthritis, and depression.[3] Living with stairs may increase the risk of fall-related injury or death. Nonfatal injuries on stairs are common in older persons and are more likely to result in hospitalization than accidents in younger people; 10% of fall-related deaths occur as a consequence of falls on stairs.[4] For older adults with no partner, managing stairs could be problematic, because many receive support in activities of daily living from their spouses.[5] This is potentially more germane for women, who tend to outlive their spouses. This study aimed to examine health-related difficulties with stairs in a large, prospective cohort study of older adults. The hypothesis was that older adults with a chronic condition and without a partner would report greater difficulty in managing stairs.

METHODS

Data were obtained from the Men, Women and Ageing (MWA) project, which incorporates data from two population-based longitudinal studies that began in 1996: the 1921 to 1926 birth cohort of the Australian Longitudinal Study on Women's Health (ALSWH) and the Perth Health in Men Study (HIMS). Detailed methods for both studies have been described elsewhere.[6,7] The human research ethics committees of the University of Newcastle and the University of Queensland approved the research protocol for the ALSWH. The ethics committee of the University of Western Australia approved the HIMS research protocol.

This analysis is based on data drawn from the fifth ALSWH survey and the third HIMS survey, both conducted in 2008. Participants in HIMS live in an urban area (Perth, Western Australia), whereas ALSWH participants are a national sample including rural and regional areas. To eliminate potential confounding related to area of residence, analyses for this study used data from ALSWH urban residents only. At the time of the 2008 surveys, the women were aged 82 to 87, and the men were aged 77 to 91. For this analysis, the age range of 82 to 87 was used for women (n = 2,421) and men (n = 1,072).

Measures

Difficulty in managing stairs was measured according to a question drawn from the Medical Outcomes Study 36-item Short Form,[8] which asks "Does your health now limit you in these activities? If so, how much: climbing several flights of stairs; climbing one flight of stairs." Responses were yes, limited a lot; yes, limited a little; or no, not limited at all.

Participants reported whether they had ever been diagnosed with any of the following chronic medical conditions: arthritis, osteoporosis, chronic obstructory pulmo-

The American Journal of Pathology, Vol. 180, No. 2, February 2012

DOI: 10.1016/j.ajpath.2011.10.031

Musculoskeletal Pathology

Antibodies against Muscle-Specific Kinase Impair Both Presynaptic and Postsynaptic Functions in a Murine Model of Myasthenia Gravis

Shuuichi Mori,* Sachiho Kubo,*
Takuyu Akiyoshi,*† Shigeru Yamada,*
Tsuyoshi Miyazaki,* Harumi Hotta,‡
Junzo Desaki,§ Masahiko Kishi,¶ Tetsuro Konishi,‖
Yuri Nishino,**††‡‡ Atsuo Miyazawa,**††‡‡
Naoki Maruyama,§§ and Kazuhiro Shigemoto*

From the Departments of Geriatric Medicine, Autonomic Nervous System,‡ and Molecular Regulation of Aging,§§ Tokyo Metropolitan Institute of Gerontology, Tokyo; the Department of Geriatric Medicine,† Graduate School of Medicine and Faculty of Medicine, the University of Tokyo, Tokyo; the Department of Integrated Basic Medicine Research,§ Ehime University School of Medicine, Ehime; the Department of Internal Medicine,¶ Toho University Sakura Medical Center, Chiba; the Department of Neurology,‖ National Hospital Organization Utano National Hospital, Kyoto; the Bio-Multisome Research Team,** RIKEN SPring-8 Center, Harima Institute, Hyogo; the Graduate School of Life Science,†† University of Hyogo, Hyogo; and Core Research for Evolutional Science and Technology,‡‡ Japan Science and Technology Agency (CREST-JST), Tokyo, Japan*

Antibodies against acetylcholine receptors (AChRs) cause pathogenicity in myasthenia gravis (MG) patients through complement pathway-mediated destruction of postsynaptic membranes at neuromuscular junctions (NMJs). However, antibodies against muscle-specific kinase (MuSK), which constitute a major subclass of antibodies found in MG patients, do not activate the complement pathway. To investigate the pathophysiology of MuSK-MG and establish an experimental autoimmune MG (EAMG) model, we injected MuSK protein into mice deficient in complement component five (C5). MuSK-injected mice simultaneously developed severe muscle weakness, accompanied by an electromyographic pattern such as is typically observed in MG patients. In addition, we observed morphological and functional defects in the NMJs of EAMG mice, demonstrating that complement activation is not necessary for the onset of MuSK-MG. Furthermore, MuSK-injected mice exhibited acetylcholinesterase (AChE) inhibitor-evoked cholinergic hypersensitivity, as is observed in MuSK-MG patients, and a decrease in both AChE and the AChE-anchoring protein collagen Q at postsynaptic membranes. These findings suggest that MuSK is indispensable for the maintenance of NMJ structure and function, and that disruption of MuSK activity by autoantibodies causes MG. This mouse model of EAMG could be used to develop appropriate medications for the treatment of MuSK-MG in humans. ***(Am J Pathol 2012, 180:798–810; DOI: 10.1016/j.ajpath.2011.10.031)***

Myasthenia gravis (MG), the most common disorder of neuromuscular synapses, is caused by autoantibodies against postsynaptic membranes at neuromuscular junctions (NMJs).[1,2] The characteristic clinical features of this autoimmune disease include ptosis, fatigue, and muscular weakness. In 2001, autoantibodies against muscle-specific kinase (MuSK) were found in 70% of patients with generalized MG who lacked antibodies to acetylcholine receptors (AChRs).[3] MuSK, a receptor tyrosine kinase, is concentrated at NMJs from the earliest stages of synaptogenesis and is required for the formation of NMJs during development.[4] Recent studies demonstrated that MuSK is activated by dimerization with low-density lipo-

Supported by grants from the Health Science Research Grants for Research on Psychiatric and Neurological Diseases and Mental Health (H19-Psycho-General-19 to K.S.), Comprehensive Research of Aging and Health (H22-Aging-General-002 to K.S.) from the Ministry of Health, Labor, and Welfare, Japan, Grants-in-Aid for Scientific Research on Innovative Area (21200023 to K.S.), Grants-in-Aid for Scientific Research (C) (21591102 to K.S.), Grants-in-Aid for Young Scientists (B) (23791009 to S.M.) from the Ministry of Education, Science, and Culture, Japan, and Intramural Research Grant (22-5 to K.S.) for Neurological and Psychiatric Disorders of National Center of Neurology and Psychiatry.

Accepted for publication October 25, 2011.

Supplemental material for this article can be found at *http://ajp.amjpathol.org* or at doi: 10.1016/j.ajpath.2011.10.031.

Address reprint requests to Kazuhiro Shigemoto, M.D., Ph.D., Tokyo Metropolitan Institute of Gerontology, Department of Geriatric Medicine, Sakaecho 35-2, Itabashi-ku, Tokyo 173-0015 Japan. E-mail: kazshige@tmig.or.jp.

protein receptor-related protein 4 (LRP4) on agrin binding to LRP4.[5,6]

We previously developed a model of experimental autoimmune myasthenia gravis (EAMG) caused by MuSK antibodies (MuSK Abs) by active immunization of rabbits with recombinant soluble MuSK protein.[7] In addition, passive transfer of human MuSK Abs from MG patients into mice was shown to cause MG.[8] These studies not only demonstrate the pathogenicity of MuSK Abs in the onset of MG, but also suggest that MuSK is required for the maintenance of mature NMJs.

Although previous studies have suggested that the disruption of NMJ maintenance by MuSK Abs might cause MG, several questions remain regarding the pathology of MuSK-MG. First, MuSK Abs in MG patients are mainly composed of the IgG4 subclass.[9,10] IgG4 antibodies do not activate the classical complement pathway, and thus cannot act through the same mechanism observed for AChR antibodies in MG.[2] Additionally, several studies have shown that small amounts of additional complement-fixing subclasses of MuSK and AChR Abs are also detectable in MuSK-MG patients,[9–11] casting doubt on the pathogenicity of MuSK Abs. Therefore, it is essential to determine whether MuSK Abs cause MG without complement activation.

Second, a number of clinical studies have shown that MuSK-MG constitutes a distinct subclass of MG. For example, patients with MuSK-MG are more prone to severe muscle weakness with respiratory crises and eventual atrophy than those with AChR-MG,[12,13] and thus require emergent and aggressive therapies. In addition, although acetylcholinesterase (AChE) inhibitors are often used effectively as symptomatic treatment for AChR-MG,[1,2] MuSK-MG patients frequently either are unresponsive to this treatment or develop cholinergic crises characterized by increasing muscle weakness.[14] A thorough understanding of the unique pathophysiology of MuSK-MG is crucial for the development and assessment of appropriate medications in the future.

To resolve this critical issue, we generated a new animal model in which 100% of mice synchronously develop EAMG after immunization with MuSK protein. This model not only reveals the pathogenic mechanisms involved in MuSK-MG, but also clarifies the role of MuSK at mature NMJs.

Materials and Methods

Preparation of Recombinant MuSK Protein

The fusion protein expression construct, consisting of the rat MuSK ectodomain and a 3′ myc/His-tag sequence, was generated as described previously.[7] 293-F cells were transfected with FreeStyle MAX reagent (Invitrogen) according to the manufacturer's instructions. Secreted recombinant MuSK protein was purified using Ni-Sepharose (GE Healthcare, Piscataway, NJ), pooled, and concentrated. The purity of the recombinant protein was determined by SDS-PAGE with Coomassie blue staining, and the concentration was determined using a Quant-iT assay kit (Invitrogen) with bovine serum albumin as a standard.

Immunization of Mice

All animal procedures used were approved by the Animal Care and Use Committee of Tokyo Metropolitan Geriatric Hospital and Institute of Gerontology. A/WySnJ and C3-deficient mice were obtained from the Jackson Laboratory (Bar Harbor, ME). A/J, B10.A-*H2*^{a}, BALB/c, and C57BL/6 mice were obtained from Japan SLC (Hamamatsu, Japan). DBA/2 and FVB/N mice were obtained from CLEA Japan (Fuji, Japan). All mice were used after 8 weeks of age. On day 0, adult female mice were anesthetized with tribromoethanol and injected subcutaneously in the hind footpads with 20 μg MuSK emulsified with complete Freund's adjuvant. All mice were boosted with 20 μg MuSK emulsified with incomplete Freund's adjuvant on day 14. All C57BL/6J and C3-deficient mice received a third injection of the same dose emulsified with incomplete adjuvant on day 28. Control mice were injected with equal volumes of PBS or equal doses of ovalbumin (OVA) emulsified with adjuvant in the same manner and on the same schedule. For comparison with MuSK-injected mice, A/WySnJ mice were injected with 20 μg AChR protein, which was purified from *Torpedo californica* as described previously[15] and emulsified with adjuvant on days 0, 14, and 42. When antigen-immunized mice exhibited a prominent cervical hump and gait disturbance, they were analyzed for EAMG.

Measurement of Muscle Strength

Forelimb muscle strength was determined by using an MK-380M grip strength meter (Muromachi Kikai, Tokyo, Japan). Mice were allowed to grip the cage lid while being held by the tail, with hindlimbs suspended, and were pulled horizontally until the grip was released. Seven measurements were performed per mouse. The highest and lowest values were discarded, and the average of the five remaining measurements was used for statistical evaluation.

Measurements of Titer and Subclasses of MuSK Antibodies

Wells of ELISA plates were coated with purified rat MuSK (150 ng/well) diluted in Tris-buffered saline. After a washing with 0.1% Tween-20/Tris-buffered saline, plates were blocked with 4% BlockAce (Dainippon Pharmaceutical, Osaka, Japan), then incubated for 3 hours at 37°C with diluted sera (1:1000 in Tris-buffered saline) from MuSK-immunized and preimmune mice. The plates were washed and then incubated for 1 hour at 37°C with HRP-conjugated antibodies against anti-mouse IgG (1:3000 in 0.1% Tween-20/Tris-buffered saline; GE Healthcare), followed by another washing and reaction with a 3,3′,5,5′-tetramethylbenzidine liquid substrate system (Sigma-Aldrich, St. Louis, MO). The colorimetric reaction was stopped by 2 mol/L HCl (2N HCl), and the values of

absorbance at 450 nm were determined as titers of MuSK antibodies. Subclasses of MuSK antibodies were determined using a Mouse Typer sub-isotyping kit (Bio-Rad Laboratories, Hercules, CA) according to the manufacturer's instructions. Only the measurement of IgE was performed by using antibody (Nordic Immunological Laboratories, Eindhoven, The Netherlands) not in the kit. In isotyping analysis, sera from MuSK-immunized mice were diluted 1:3000.

Electromyography

Changes in compound muscle action potential (CMAP) were studied using a PowerLab 4/26 data acquisition system (ADInstruments, Colorado Springs, CO). Mice were anesthetized with tribromoethanol and maintained at 37°C on a thermoregulation device. Paired stimulating electrodes separated by 2 to 3 mm were inserted intramuscularly near the sciatic notch for supramaximal stimulation at 3 Hz. Recording electrodes were inserted in the medial compartment of the gastrocnemius muscle and near the insertion of the Achilles tendon. To isolate stimulus artifacts, a ground electrode was placed between the stimulus and recording electrodes. Decrement was calculated as percent amplitude change between the first and least CMAPs evoked by a train of 10 impulses. If the amplitude of the first CMAP was the least within the measurement, the decrement was designated as 0%. In drug treatment experiments, neostigmine bromide (37.5 μg/kg; Sigma-Aldrich) was given by intraperitoneal injection. A typical mouse weighing 20 g received 100 μL of freshly prepared solution containing 7.5 μg/mL of neostigmine bromide in PBS. After 20 minutes, the effect of drug treatment was evaluated via electromyography (EMG).

In Vitro *Electrophysiology*

Left phrenic nerve and hemi-diaphragm muscle preparations were made after tribromoethanol anesthetization. The muscle specimen was placed in a 1.0-mL chamber filled with Tyrode's solution, which was constantly oxygenized by a gas mixture of 95% O_2/5% CO_2 released close to the fluid surface. Membrane potentials and miniature endplate potentials (MEPPs) were recorded at room temperature (18°C to 22°C) using a glass microelectrode filled with 3 mol/L KCl via a PowerLab 4/26 data acquisition system. To measure evoked endplate potentials (EPPs), μ-conotoxin GIIIB (Peptide Institute, Osaka, Japan) was added to the chamber (1 μmol/L final concentration) to suppress muscle contraction, and the phrenic nerve was stimulated by silver electrodes with supramaximal voltage at 0.7 Hz. Amplitudes of EPPs and MEPPs were standardized to a membrane potential of −75 mV. Quantal content was calculated by applying the values of mean MEPP amplitude, mean EPP amplitude, and membrane potential in the same muscle fiber to a formula reported previously.[16,17] To analyze rate of EPP decay, an exponential function was fitted to the falling phase portion from 80% to 20% of EPP peak value, and the decay time constant (τ) was calculated using the Peak Parameter program in the LabChart software package (version 7.1.2; ADInstruments). The MEPP frequency was calculated from a >1 minute recording in each NMJ. To exclude the effects of μ-conotoxin treatment and nerve stimulation on spontaneous neurotransmission, frequency measurements were performed separately from those of quantal content. Data for ≥10 NMJs were obtained from each normal or MuSK-immunized mouse.

Whole-Mount Staining of NMJs

For quantification of nerve terminals and AChR and AChE staining areas, whole-mount staining of soleus muscles was performed. Soleus muscles were removed and fixed in 1% paraformaldehyde/PBS for 10 minutes at room temperature, rinsed in PBS, and incubated with 0.1 mol/L glycine/PBS. After filleting muscles into several sheets of fibers using microdissection scissors, muscle slices were incubated with either rhodamine or Alexa Fluor 647-conjugated α-bungarotoxin (BTx, 40 nmol/L in PBS; Invitrogen) to label AChRs for 1 hour at room temperature. Muscles were then rinsed in PBS, permeabilized in methanol at −20°C, washed again in PBS for 30 minutes, and blocked for 1 hour in 2% bovine serum albumin/0.3% TritonX-100/PBS. Slices were then incubated overnight at 4°C in a cocktail of primary antibodies diluted in blocking solution. Axons and nerve terminals were labeled with rabbit polyclonal antibodies against neurofilament (1:400; Millipore-Chemicon International, Temecula, CA) and synaptophysin (1:100; Invitrogen).

For quantification of nerve terminals, muscles were incubated only with anti-synaptophysin. Rabbit polyclonal antibody against AChE (1:1000) was generated by Dr. Terrone L. Rosenberry (Mayo Clinic College of Medicine). Antiserum against collagen Q (ColQ, 1:2000) was prepared by injecting Wistar rats with a synthetic peptide corresponding to residues 35 to 51 of the ColQ deduced primary sequence coupled to keyhole limpet hemocyanin. After incubation with primary antibodies, muscles were rinsed three times (20 minutes each) in PBS and incubated overnight at 4°C with either Alexa Fluor 488- or Alexa Fluor 555-conjugated secondary antibodies (1 μg/mL in blocking solution; Invitrogen) corresponding to the hosts of the primary antibodies. After incubation with secondary antibodies, muscles were rinsed three times (20 minutes each) in PBS and flat-mounted in a SlowFade antifade kit (Invitrogen) for confocal microscopic analysis. For quantification of AChR staining intensity, diaphragms were dissected and fixed in 1% paraformaldehyde/PBS for 1 hour at room temperature, rinsed in PBS, and incubated with 0.1 mol/L glycine/PBS. Some pieces of left hemi-diaphragm were incubated overnight at 4°C with Alexa Fluor 488-BTx (40 nmol/L in PBS; Invitrogen). Muscles were then rinsed three times (20 minutes each) in PBS and flat-mounted in the same way as soleus muscles. Confocal images were acquired with a Leica TCS SP5 confocal laser scanning unit, using a 63× glycerin objective on a Leica DMI6000 microscope (Leica Microsystems, Wetzlar, Germany), and images of ≥30 NMJs were acquired from each control or MuSK-immunized

mouse (n = 3 mice/group). For quantification of synaptophysin, AChR and AChE staining areas were quantified on a maximum projection of confocal images with ImageJ software (version 1.42q; NIH, Bethesda, MD). The ImageJ Analyze Particle program was used to quantify the areas of each staining experiment.

Electron Microscopy

After tribromoethanol anesthetization, tibialis anterior muscles were exposed and fixed *in situ* with 4% glutaraldehyde/0.1 mol/L phosphate buffer at pH 7.3 for 5 minutes. Muscles were then dissected, cut into small strips, postfixed with the same solution for 2 hours at room temperature, rinsed several times in distilled water, and further postfixed with 1% unbuffered osmium tetroxide for 30 minutes. For SEM observation, muscles were treated with a HCl-hydrolysis procedure to remove intramuscular connective tissues as described previously.[18] After a drying via the critical point method and then a sputter coating with platinum, specimens were examined in a Hitachi S-800 SEM (Hitachi High-Technologies, Tokyo, Japan). For TEM observation, diaphragms were fixed *in situ* by injecting the fixative intrathoracically and intraperitoneally until these cavities were filled. Small pieces of fixed muscle were block-stained with 3% aqueous uranyl acetate for 2 hours and embedded in Epon 812 resin (Nissin EM, Tokyo, Japan) after dehydration through an ethanol series. Ultrathin sections were cut with an Ultracut E ultramicrotome (Reichert-Jung, Austria), doubly stained with uranyl acetate and lead citrate, and then examined with a Hitachi HU-12A transmission microscope (Hitachi High-Technologies). For morphometric analysis, TEM images were scanned and the density of junctional folds was determined by the number of folds divided by the length of the presynaptic membrane using ImageJ software (version 1.42q). Images of ≥10 NMJs from each mouse were obtained for quantification.

Preparation of IgG Fractions and Fab Fragments from MuSK Antisera

Sera from MG-affected mice were collected, and the IgG fraction was purified with Protein G-Sepharose (GE Healthcare) as anti-MuSK IgG. Fab fragments of anti-MuSK IgG were prepared using a Pierce mouse IgG1 Fab preparation kit (Thermo Scientific, Rockford, IL) with papain digestion. As a control, IgG fractions (normal IgG) and Fab fragments (normal Fab) were prepared from sera of preimmune mice using the same method.

AChR Clustering Assay

The C2C12 cell line was obtained from the American Type Culture Collection (ATCC, Manassas, VA) and used for three to eight passages. Cells were cultured in 12-well plates as myoblasts in 10% fetal calf serum (FCS)/Dulbecco's modified Eagle's medium. When the cells reached confluency, myotube formation was induced by replacing the medium with 2% horse serum/Dulbecco's modified Eagle's medium. The cells were incubated for 3 days, with fresh medium exchange every day, until full differentiation into multinucleated myotubes was observed morphologically. Preparation of recombinant agrin protein was as described previously.[7] Myotubes were treated with 10 μg/mL anti-MuSK IgG or Fab for 30 minutes, and then incubated for 16 hours with 1 nmol/L agrin. AChR clustering was visualized after incubation with 40 nmol/L Alexa Fluor 594-BTx (Invitrogen) in fusion medium for 1 hour at 37°C before fixation. Fluorescence images of myotubes were acquired using a 20× objective on a Leica DMI6000 microscope; the number of AChR clusters in six randomly selected fields was counted.

MuSK Phosphorylation Assay

The C2C12 myotubes were treated with either 10 μg/mL anti-MuSK IgG or Fab. After 30 minutes, half of the myotube cultures were further treated for 30 minutes with 1 nmol/L agrin, and the remaining cultures were left untreated. The myotubes were lysed and solubilized using a protease inhibitor cocktail (complete EDTA-free; Roche Applied Science, Indianapolis, IN) with 2 mmol/L sodium orthovanadate. Extracts were immunoprecipitated with antibodies directed against MuSK, and the resulting precipitates were immunoblotted with either a mixture of the anti-phosphotyrosine antibodies 4G10 (Millipore, Billerica, MA) and PY20 (Millipore-Chemicon International) or MuSK antibodies. Antibodies directed against MuSK were generated in rabbits as described previously.[7] Band intensities of immunoblots were assessed using ImageJ software (version 1.42q).

Statistical Analysis

Significant differences between control and MuSK-injected mice were analyzed by unpaired t-test. Paired t-test was used to analyze the effect of neostigmine treatment in EMG experiments. Analysis of variance was used to assess AChR clustering and MuSK phosphorylation assays. P values of <0.05 were considered statistically significant.

Results

MuSK Protein Injection Results in Synchronous Muscle Weakness with Weight Loss

A/WySnJ mice were injected with 20 μg of MuSK protein on days 0 and 14 of the experiment. Because A/WySnJ mice carry mutations that result in C5 deficiency,[19] these mice cannot generate a lytic membrane attack complex and are therefore highly resistant to EAMG after AChR immunization.[20,21] All mice (n = 18) injected with MuSK manifested severe muscle weakness with tremors within 2 weeks of the second injection. These symptoms occurred synchronously in all animals, along with the appearance of a prominent cervicothoracic hump, indicat-